Available online at www.sciencedirect.com
ScienceDirect
International Journal of Mass Spectrometry 271 (2008) 8–14
International Journal of Mass Spectrometry
www.elsevier.com/locate/ijms

Absolute partial photoionization cross sections of ozone☆

J. Berkowitz *

Argonne National Laboratory, Chemistry Division, 9700 South Cass Avenue, Argonne, IL 60439, USA

Received 19 September 2007; received in revised form 8 November 2007; accepted 13 November 2007
Available online 22 November 2007

Dedication: To Dr. Yong-Ki Kim, a close friend, a true gentleman, and a very good scientist.

Abstract

Despite the current concerns about ozone, absolute partial photoionization cross sections for this molecule in the vacuum ultraviolet (valence) region have been unavailable. By eclectic re-evaluation of old/new data and plausible assumptions, such cross sections have been assembled to fill this void.

Keywords: Non-Koopmans orbitals; Ionic states; Ionization and appearance potentials; Parent and fragment ions; Partial cross sections

1. Introduction

The ozone molecule (O_3) has C_{2v} symmetry in its electronic ground state, with an equilibrium bond angle of 116.78° and r_e(O–O) = 1.2717 Å (Colmont et al.) [1]. Ozone in its ground state is not well described by a single configuration, due to its biradical character (Hay et al.) [2]. The core molecular orbitals (MOs) are unambiguously (in C_{2v}) $1a_1^2\ 2a_1^2\ 1b_2^2$. The innermost ($1a_1$) is identified with the central O1s atomic orbital (AO), while $2a_1$ and $1b_2$ are even and odd combinations of the terminal O1s AOs. The inner valence orbitals $3a_1^2\ 2b_2^2\ 4a_1^2$ are derived from O2s AOs. To succinctly describe the outer valence orbitals (composed of O2p AOs) two configurations are necessary (Laidig and Schaefer, 1981) [3].

$$\Phi_1 = \ldots 5a_1^2\ 3b_2^2\ 1b_1^2\ 6a_1^2\ 4b_2^2\ 1a_2^2\ (\sim 77\%)$$
$$\Phi_2 = \ldots 5a_1^2\ 3b_2^2\ 1b_1^2\ 6a_1^2\ 4b_2^2\ 2b_1^2\ (\sim 23\%)$$

Here, the $5a_1$ and $3b_2$ MOs have σ bonding character, the $6a_1$ and $4b_2$ formally the same but essentially lone pairs on the terminal oxygen atoms. The $1b_1$ is a π (out of plane) orbital primarily situated on the central oxygen, while the $1a_2$ and $2b_1$ (which are the defining features of the Φ_1 and Φ_2) are combinations of pπ orbitals from the terminal oxygen atoms (Stranges et al.) [4]; (Mason et al.) [5]. In addition, the three lowest unoccupied molecular orbitals (LUMOS) are $2b_1$ (the π* antibonding complement to $1b_1$), $7a_1$ and $5b_2$, both σ* (antibonding).

Perhaps the most significant photoexcitation in O_3, known as the Hartley band, has a high cross section between 2100 and 3000 Å with a maximum of 11.73 Mb at 2555 Å (4.85 eV) which absorbs most of the deep UV radiation (below 3000 Å) before the air cutoff. It is attributed to an $\tilde{X}^1A_1 \rightarrow {}^1B_2$ excitation, where the configuration of $^1B_2$ is $\ldots (1a_2)^1(2b_1)^1$, intimately connected with the two configuration description of the ground state [2,5]. The absorption of solar radiation by ozone in the stratosphere by this transition controls the penetration of higher energy ultraviolet rays of the earth's surface (Molina and Molina) [6], but not the familiar UVA and UVB bands which mostly span the 3000–4000 Å region. It also leads to its destruction by photodissociation (Takahashi et al.) [7] requiring its reconstitution by further chemical processes.

The fear of its destruction by other chemical processes has motivated theorists and experimentalists to examine the electronic and chemical behavior of ozone. Our interests here are the ionization properties, which currently are still in a state of limbo.

* Tel.: +1 630 252 4086; fax: +1 630 252 9647.
E-mail address: berkowitz@anl.gov.

1387-3806/$ – see front matter © 2007 Elsevier B.V. All rights reserved.
doi:10.1016/j.ijms.2007.11.005

2. Absolute cross sections, outer and inner valence orbitals

Fig. 1 is a recent photoelectron spectrum of ozone in the valence region, taken with 100 eV incident synchrotron radiation (Wiesner et al.) [8]. It does not differ greatly from earlier spectra. In fact, the insert is adapted from a portion of a He I photoelectron spectrum from Katsumata et al. [9]. The spectrum of Fig. 1 is comparable in resolution to earlier work, has avoided the presence of extraneous resonance lines common to discharge light sources, and has apparently suppressed O_2 impurities. Its essential features have been known since the 1970s. Nevertheless, the interpretation continues to present a challenge.

There appears to be general agreement that the features between ~12.5 and 14 eV contain the lowest three ionization energies. Koopmans' theorem calculations predict the order $^2A_2$ (13.43 eV) < $^2A_1$ (15.28 eV) < $^2B_2$ (15.77 eV) (Dyke et al.) [10]; Hay et al. [2]. The most extensive calculations place the order $^2A_1 < {}^2B_2 < {}^2A_2$, with the lowest two almost degenerate, forming a conical intersection in the Franck–Condon region (Schmelz et al.) [11]; Müller et al. [12]; McKeller et al. [13]. The ionized state with a hole in the $1a_2$ orbital is actually the third lowest state. This circumstance has prompted Kosugi et al. [14] to dub this a "double breakdown" of Koopmans' theorem, since the theorem predicts the third state to be the first. Kosugi et al. [14] have also ventured beyond the lowest three ionization energies and offered a rationale for the relative weakness and profusion of higher energy states. By including initial state and final state configuration interaction (ISCI and FSCI), and calculating monopole intensities, as is often done with core-electron excitation, they show that whereas the primary ionization is 81.1% ($6a_1$), 73.1% ($4b_2$) and 75.2% ($1a_2$), it drops to ~40% for $2b_1$ and $1b_1$ (which are mixed) and remains <50% for the other valence orbitals. In other words, the requirement of a multiconfiguration description of the ground state has vitiated a Koopmans' theorem portrayal and instead has fostered a description of the outer valence orbitals of O_3 similar to that reserved for the inner valence orbitals of other molecules.

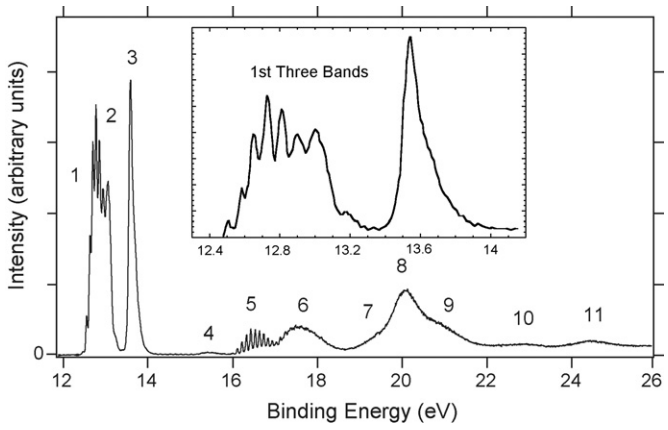

Fig. 1. The photoelectron spectrum of ozone measured with 100 eV photons (from Wiesner et al. [8]). Inset: expanded view of the first three bands, from a He I (21.2 eV) photoelectron spectrum (from Katsumata et al. [9]).

The most recent experimental measurements of valence energies for O_3 appear to be those of Wiesner et al. [8], photoelectron spectroscopy (PES) with 100 eV incident radiation, Couto et al. [15], threshold photoelectron spectroscopy (TPES), and Willitsch et al. [16], pulsed field ionization, zero electron kinetic energy spectroscopy (PFI-ZEKE). Of these, the latter offers the highest precision, with rotational resolution. The adiabatic IP for $\tilde{X}^2A_1$ is found to be 12.52495(6) eV, which is in satisfactory agreement with an older photoionization mass spectrometric value of 12.519(4) eV (Weiss et al.) [17], but discounts a hot band at 12.44 eV found by Dyke et al. [10], Katsumata et al. [9] and Wiesner et al. [8]. The rotational analysis leads to a structure of $\tilde{X}^2A_1$ with $r_0 = 1.25$ Å and a bond angle of 131.5°, which suggests excitation of bending vibrations upon ionization. The vertical IP (see Fig. 1) appears to correspond to the (0 3 0) level of $\tilde{X}^2A_1$, and from the energies given by Willitsch et al. amounts to 12.7500 eV, while the (0 0 0) level of $\tilde{A}^2B_2$ is found by them at 12.66004(7) eV i.e., between (0 1 0) and (0 2 0) of the $\tilde{X}^2A_1$ state. Only this one bound vibrational level could be identified for the $\tilde{A}^2B_2$ state. Rotational analysis of this band yields $r_0 = 1.37$ Å and a bond angle of 111.3°, which favors excitation of the symmetric stretch upon ionization. At higher energies, they encountered strong spectral congestion, but some partially resolved rotational features enabled them to conclude that these bands had smaller rotational constants, suggesting that a large and abrupt change in the O_3^+ geometry was taking place. The observation of an isolated vibronic state ($\tilde{A}^2B_2$) at 12.66 eV differs from that of Katsumata et al. shown in Fig. 1 and indeed of most other researchers (e.g. Katsumata et al. [9], Wiesner et al. [8], Couto et al. [15]), who placed the vertical value at 13.00 eV. Willitsch et al. have performed ab initio calculations in support of their experimental observations which show a crossing between $\tilde{X}$ and $\tilde{A}$ states at ~12.73 eV in C_{2v} symmetry which is avoided in C_s symmetry (unequal O–O distances), leading to saddle points and barriers connecting $\tilde{X}$ and $\tilde{A}$ states in regions of large intermolecular distances, which may rationalize the spectral congestion and low rotational constants noted at higher energy. The flat and anharmonic potential is underscored by the low dissociation of energy of O_3^+, 0.6 eV (Weiss et al. [17]; Moseley et al. [18]; Willitsch et al. [16]).

It may not have gone unnoticed by the reader that the only vibrational state of $\tilde{A}^2B_2$ identified by Willitsch et al. at 12.66004(7) eV, is very close to (0 2 0) of $\tilde{X}^2A_1$ at 12.6762 eV. Although clearly distinguishable in their PFI-ZEKE spectrum, these two peaks are merged in Fig. 1. Also, Willitsch et al. have reported the positions of five vibrational bands (0 0 0) to (0 4 0) of the $\tilde{X}^2A_1$ state, but the two peaks of the highest energy in the 12.5–13.0 eV cluster are unaccounted for. Perhaps this can best be rationalized at the present time by a calculation performed by Müller et al. [12], which was the culmination of earlier work. These authors vibronically coupled the $\tilde{X}^2A_1$ and $\tilde{A}^2B_2$ states, and used diabatic potential surfaces. With some modeling, they were able to reproduce the first three peaks ($\Delta E \sim 0.01$ eV, relative intensity 10^{-2}) and to show the presence of the higher energy peaks due to strong nonadiabatic mixing of vibrational levels of the $\tilde{X}$ and $\tilde{A}$ states. Willitsch et al. also allude to this

interpretation, but call for calculations of spectroscopic accuracy.

Returning now to an interpretation of Fig. 1, we allude to recent configuration interaction (CI) calculations by Ohtsuka et al. [19]. Similar results were reported earlier by Decleva et al. [20]. In the spirit of Katsumata et al. [9], they calculate the energies and monopole intensities of 57 states of O_3^+ between the first IP and 28 eV. In agreement with Katsumata et al. and most recent work, the strongest transitions are to the lowest three states $\tilde{X}^2A_1$, $\tilde{A}^2B_2$, $\tilde{B}^2A_2$ (peak 3 at 13.54 eV). Each is primarily a single hole state, with monopole intensity (MI) of ∼0.7. Peak 4 at 15.6 eV (15.4 eV, Wiesner et al. [8]) is a two-hole, one particle ($6a_1^{-1}2b_1\ 1a_2^{-1}$ [$^2B_2$]) state and is correspondingly weak (MI ∼ 0.01) (see also Decleva et al. [20]), as are most of the remaining peaks. The other single-hole states are the vibrationally structured peak 5 (AIP = 15.95 eV, VIP = 16.09 eV) which shares its $(1b_1)^{-1}$ character with peak 9 (VIP = 20.9 eV), peak 6 $(5a_1)^{-1}$, VIP = 17.60 eV, and two states with $(3b_2)^{-1}$ character contributing to peak 8 (VIP = 20.1 eV). The shoulder at 19.4 eV shown as peak 7 in Fig. 1 is calculated by Ohtsuka et al. [19] to be a three-hole, two-particle state, while there are several candidates of the two-hole, one-particle type (Ohtsuka) which can be identified with the broad and weak structures marked 10 and 11. These assignments are summarized in Table 1. Not appearing in Fig. 1, but barely visible in the He II spectrum of Katsumata et al. [9] is a single-hole component of the inner valence $(4a_1)^{-1}$ at 26.8 eV. Decleva et al. [20] calculate two dominant configurations having $(4a)^{-1}$ character for this energy region with relative intensities of ∼0.17 and ∼0.11 on their scale, but at higher energy "a real shattering of the O_{2s} shell is apparent, the highest $2b_2$ and $3a_1$ intensities being 0.076 and 0.056, respectively, with only a few more lines above 0.04 spectral strength." They conjecture that this behavior is more extensive than the oft-encountered breakdown of the one-particle picture for inner shell ionization, being close to an unstructured continuum. Experimental data are unavailable. Decleva et al. find that $(2b_2)^{-1}$ has larger contributions at ∼33 and ∼37.5 eV, and $(3a_1)^{-1}$ at ∼40 eV. Padial et al. [21], recognizing that configuration mixing is important for inner-valence-shell ionic states, restrict themselves to Koopmans' theorem values of 29.86 eV ($4a_1^{-1}$), 39.58 eV ($2b_2^{-1}$) and 48.55 eV ($3a_1^{-1}$).

To the best of our knowledge, there have been no reported measurements on the energy dependence of the partial cross sections or branching ratios corresponding to the ionic states shown in Fig. 1 and discussed in the preceding section. Padial et al. [21] have performed calculations of partial and total photoionization cross sections as a function of excitation energy from 13 to 55 eV employing Stieltjes–Tchebycheff techniques and the separated-channel static-exchange approximation. We are unaware of any other calculation of partial cross sections for O_3. Fig. 2 is a reproduction of their results. It is fair to ask for experimental tests of this calculation. Decleva et al. [20] have examined the ratio between $\sigma(1a_2^{-1})$ (3 in Fig. 1) and the combined $\sigma(6a_1^{-1} + 4b_2^{-1})$ (1 + 2 in Fig. 1). They find that this ratio changes from 1.5 at 21.2 eV to 0.75 at 40.8 eV in the calculations of Padial et al., an enhancement of a factor of 2 for $\sigma(6a_1^{-1} + 4b_2^{-1})$ over $\sigma(1a_2^{-1})$. The He I and He II photoelectron spectra display a similar trend,

Table 1
A current CI interpretation of valence shell PES

Band no.[a]	1 + 2	3	4	5	6	7	8	9	10	11
Relative intensity[b]	2.05	1.00	0.015	0.083	0.474		0.912		0.018	0.05
Major configuration[c]	$0.80(6a_1^{-1}) + 0.78(4b_2^{-1})$	$0.9(1a_2^{-1})$	2h-1p	$0.34(1b_1^{-1})$	$0.39(5a_1^{-1})$	3h-2p	$0.36(3b_2^{-1}) + 0.59(3b_2^{-1})$	$0.56(1b_1^{-1})$	2h-1p	2h-1p

[a] Refer to Fig. 1.
[b] Intensities based on areas under bands.
[c] From calculations of Ohtsuka et al. [19].

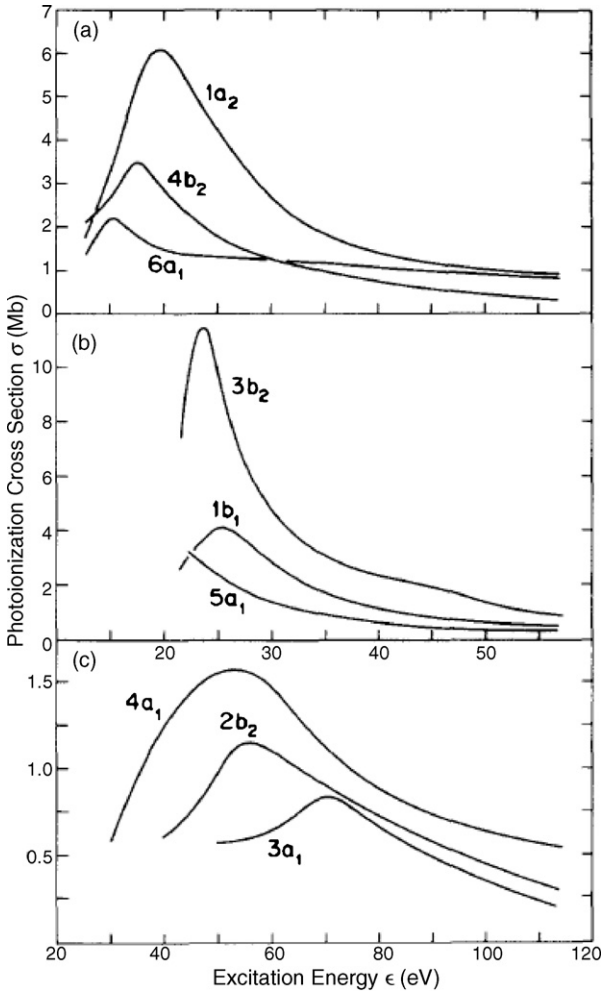

Fig. 2. Energy dependence of the absolute partial photoionization cross sections of valence orbitals in ozone, as calculated by the Stieltjes–Tchebycheff technique and the separated-channel static-exchange approximation (from Padial et al. [21]). (a) Outer valence shells $6a_1$, $4b_2$, and $1a_2$; (b) $1b_1$, $3b_2$, and $5a_1$; (c) inner valence shells $4a_1$, $2b_2$ and $3a_1$, with a different energy scale.

providing support (though limited) for the calculation. Another test is the spectral dependence of the total photoionization cross section. We have summed the partial cross sections shown in Fig. 2, and compared them with a patchwork of experimental total photoionization cross sections in Fig. 3. Cook [22,23] used a 50 cm absorption cell with parallel plates extending the length of the cell to make absolute photoionization (and photoabsorption) cross section measurements. The spectra he presented in 1970 indicated that the quantum yield of ionization is approaching unity at 600 Å ≡ 20.66 eV but his absolute scale of cross sections [23] had been reduced from his original calibration [22]. Using his 1968 calibration, which is preferred by sum rule analysis [24], leads to an enhancement in cross section by a factor 1.4 which has been used in constructing Fig. 3. The electron energy loss (EELS) spectral intensities of Celotta et al. [25] have been normalized to those of Cook (revised) at 20.5 eV and Ogawa and Cook [26] from 20.5 to 23.5 eV, and scaled by E^2 (found empirically to fit the photoabsorption data at this energy) up to 30.3 eV, where $h\nu = E > 21$ eV. Here, we have implicitly assumed

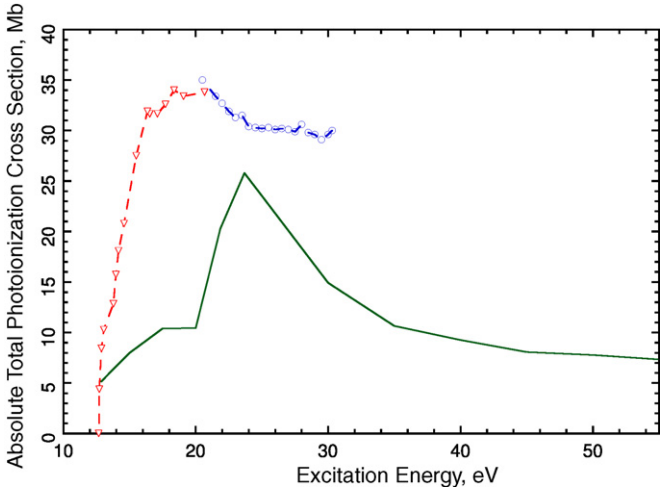

Fig. 3. Spectral dependence of the absolute total photoionization cross section of ozone in the valence region. (—) Sum of calculated partial cross sections, Padial et al. [21]; (▽) Cook [23], normalized to sum rules and to Cook [22]; (◯) electron energy loss data of Celotta et al. [25] normalized to photoabsorption data of Cook (revised) and Ogawa and Cook [26] above 20.5 eV and scaled by E^2.

that photoabsorption and photoionization cross sections can be taken to be the same for $h\nu > 21$ eV.

In Fig. 3, the calculated total photoionization cross section has a distinct, broad peak centered at ~23.7 eV, which is absent in the patched experimental data. Interestingly, Padial et al. [21] comment that the "total calculated photoionization cross section in the ~22–30 eV interval is seen to be monotonic and structureless, in general accord with photoabsorption and electron-impact measurements." None of the references cited there for photoabsorption cover this energy range, and the electron impact measurement cited is the one we have used. The peak in the calculations can be traced to a $3b_2(n) \rightarrow 5b_2(\sigma^*)$ resonance at ~23 eV described by Padial et al. but as yet unsupported by experimental evidence.

It is difficult to judge the quantitative accuracy of Fig. 2. The same theoretical methods were used by the same authors (Padial et al. [27]) on CO_2, where the results could be compared with experimental data, and they were "in very good quantitative accord." [27]. However, in O_3 one should incorporate the biradical nature of the ground state, the effects of configuration interaction, determination of shake-up amplitudes, etc. which the authors have acknowledged neglecting in this case. The extreme departure from independent particle behavior, in which satellites appear in the outer valence region (usually encountered in the inner valence region), while the inner valence region is so shattered that it approaches an unstructured continuum [14,20,19] is likely to have limited the accuracy of the calculation of Padial et al. [21].

3. Photoionization mass spectrometry: absolute partial cross sections of ions, valence region

The ion energetics of ozone is well established. The adiabatic IP(O_3) is 12.52495(6) eV, as noted earlier (Willitsch et al. [16]). The appearance potential for O_2^+ (O_3) can be

inferred from the dissociation energy of O_3 into $O(^3P_2)$ and O_2 ($X^3\Sigma g^-$) given as 24.49(1) kcal/mol = 1.0621(4) eV (Taniguchi et al. [28]) and the IP(O_2) of 12.07014(15) eV (Merkt et al. [29]) to be 13.1322(4) eV, and AP $O^+(O_3)$ from IP(O) of 13.618055(7) eV (Moore [30]) to be 14.6802(4) eV. Decomposition into three particles ($2O + O^+$) has a thermochemical threshold of 19.7668(2) eV. Doubly charged ozone (O_3^{2+}) appears to be unstable on a microsecond time scale (Newson and Price [31]); decomposition into O_2^+ and O^+ is initially observed at ~34.3 eV, though the asymptotes (far beyond the Franck–Condon region) are 26.75 eV (triplet) and 30.07 eV (singlet).

Surprisingly, only two photoionization mass spectrometric studies of ozone in the valence region have been reported (Weiss et al. [17]; Mocellin et al. [32]) (a third by Cook [23] alluded to earlier, was performed at too high a pressure, and apparently intended for ion-molecule studies). The investigation by Weiss et al. utilized a magnetic sector mass spectrometer, which had the relative advantage of higher photon resolution (5–10 meV) and a better signal-to-noise ratio, despite the fact that the light source employed was a laboratory discharge. However, it was likely to discriminate against fragment ions possessing significant kinetic energy. The experiment reported by Mocellin et al. employed a time-of-flight (TOF) spectrometer, which was less likely to discriminate against fragment ions (they measured ~0.25–0.3 eV for O_2^+, ~1.3–1.4 eV for O^+), but the photon energy resolution was poorer (20–40 meV), and there was a significant background from scattered synchrotron light. Both investigations measured relative ion yields. To convert to absolute partial cross sections, some absolute calibration was required.

Before turning to these calibrations, we note that Weiss et al. obtained IP(O_3) of 12.519(4) eV whereas Mocellin et al. identified "a weak adiabatic production at 12.7 eV." Also, Weiss et al. deduced an AP $O_2^+(O_3)$ of 13.125(4) eV at 0 °K by linear extrapolation and thermal correction, compared to the thermochemical threshold of 13.1322(4) eV, whereas Mocellin et al. observed a "rise in the O_2^+ production . . . at 13.2 eV." For O^+, which is very weak near threshold, Weiss et al. detected initial departure from a linear background at 15.21(1) eV, ca. 0.53 eV above the thermochemical threshold, while Mocellin et al. see no "clear structures" in the ion yield curve, apart from a "most evident . . . increase after 18.3 eV."

In addition to the relative ion yields of O_3^+, O_2^+, and O^+, Mocellin et al. present the total ion yield (TIY) from threshold to 22 eV, which should be comparable to the total photoionization cross section of Cook (see Fig. 3) when both are normalized at ~21 eV. However, the total cross section of Cook starts steeply and begins to level off at ~16.5 eV, whereas the TIY of Mocellin et al. achieves 2/3 of its growth above 17 eV.

For absolute calibration of ozone photoionization cross-sections, we have little choice. Cook's figure can be viewed in Ref. [23]. In the article, mention is made of a previous report [22], though the latter contains no figure, and the available abstract mentions little about ozone other than a maximum in the photoabsorption cross section of 42 Mb at 725 Å. That datum is about 40% higher than shown in the 1970 figure, as previously noted. However, the relationship of the absolute photoionization curve to the absolute photoabsorption curve in Cook's 1970 figure is plausible. There is an abrupt rise at the IP, and the quantum yield of ionization does not exceed unity, though it appears to gradually approach this value at 600 Å (20.66 eV). As a working hypothesis, we have used Cook's 1970 curve, increased by ~40%, as the absolute total photoionization cross section of ozone.

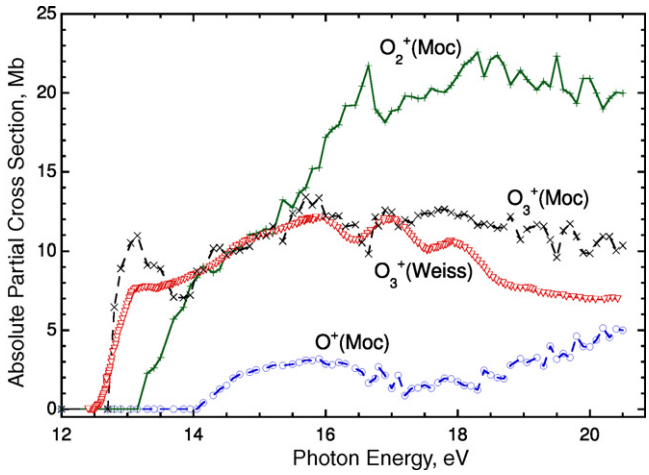

Fig. 4. Absolute photoionization cross sections for formation of O_3^+, O_2^+, and O^+ from ozone, using branching ratios extracted from relative ion yields of Mocellin et al. [32] and the absolute total photoionization cross section of Cook [22,23]. Also shown, on an arbitrary scale, is the relative ion yield of $O_3^+(O_3)$ taken directly from Weiss et al. [17]. The parent ion O_3^+ is formed with thermal kinetic energy and can be directly compared in the two experiments, whereas the fragment ions O_2^+ and O^+ have significant kinetic energy. (+—+) O_2^+ (Mocellin et al. [32]); (x—x) O_3^+ (Mocellin et al. [32]); (▽) O_3^+ (Weiss et al. [17]); (◯) O^+ (Mocellin et al. [32]).

Since discrimination against fragment ions is less likely in the TOF experiments of Mocellin et al. we have converted their relative ion yields to branching ratios, and applied them to the modified total photoionization cross section of Cook. The resulting absolute partial cross sections of O_3^+, O_2^+, and O^+ are shown in Fig. 4. They reveal that $\sigma(O_2^+/O_3)$ becomes comparable to $\sigma(O_3^+/O_3)$ between ~14 and 15.5 eV, and becomes about double the parent ion by ~20–21 eV. The $\sigma(O^+/O_3)$ will be discussed shortly. Also shown in Fig. 4 is the relative ion yield of O_3^+ from Weiss et al. (which should not be subjected to kinetic energy discrimination) roughly normalized to the absolute $\sigma(O_3^+/O_3)$ deduced from the data of Mocellin et al. at one energy. They have not been normalized to the Cook cross sections.

In comparing the two parent ion curves, we see some welcome similarities. The steep increase from the threshold (12.52–13.1 eV) corresponds to the intermingled peaks 1 and 2 in the PES of Fig. 1, which we shall refer to as $(6a_1)^{-1} + (4b_2)^{-1}$. They constitute about 45% of the intensity (area) in Fig. 1, and it does not change dramatically between He I (21.2 eV), He II (40.8 eV) and 100 eV incident energy. Between 13.1 and 13.5 eV, $\sigma(O_3^+/O_3)$ is flat (Weiss) or decreases (Mocellin) while $\sigma(O_2^+/O_3)$ begins its ascent. Starting at about 13.5 eV, corresponding to peak 3 in Fig. 1, and extending to ~16 eV photon energy, there appears to be a significant increase in the parent ion intensity. This is unexpected because in standard quasi-equilibrium theory (QET) any increase in the parent ion should

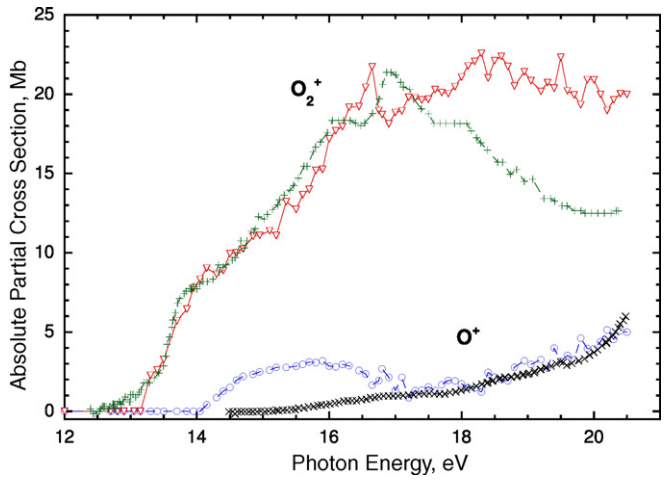

Fig. 5. Absolute partial cross sections of $O_2^+(O_3)$ and $O^+(O_3)$ derived from Mocellin et al. [32] as in Fig. 4, compared with $O_2^+(O_3)$ from Weiss et al. [17] with its relative ion yield multiplied by 2.5, and $O^+(O_3)$ from Weiss et al. [17], relative ion yield multiplied by 5. (▽) O_2^+ (Mocellin et al. [32]); (+) O_2^+ (Weiss et al. [17], RIY × 2.5); (◯) O^+ (Mocellin et al. [32]); (x) O^+ (Weiss et al. [17], RIY × 5.0).

cease with the appearance of the first fragment. This experimental result may not be as apparent in the $\sigma(O_2^+/O_3)$ of Mocellin et al. but they unmistakably refer to a large band in the partial ion yield spectrum of O_3^+ between 15.4 and 16.5 eV. They attribute this increase to peak 4 in Fig. 1, which seems unlikely since its contribution to the photoelectron spectrum is only 0.3%.

A better view of $\sigma(O_2^+/O_3)$ and $\sigma(O^+/O_3)$ can be seen in Fig. 5, where the data of Mocellin et al. are repeated, but the relative fragment intensities of O_2^+ and O^+ from Weiss et al. have been increased by factors of 2.5 and 5, respectively, to take into account their kinetic energies. These are arbitrary factors, but they illustrate the similarities in the results of the two experiments, which thereby acquire a veneer of plausibility, and the differences, which require explanation. The two $\sigma(O_2^+/O_3)$ figures mostly track one another, but at high energy (17–20 eV) the Weiss data decline while the Mocellin data remain roughly flat. A similar observation can be made for $\sigma(O_3^+/O_3)$ in Fig. 4. A possible explanation is a photoelectric correction for the measurements of light intensity in the data of Weiss et al. Returning to Fig. 5, we can see a distinct increase in slope for $\sigma(O_2^+/O_3)$ at 13.5 eV particularly in the Weiss data, which signal the onset of $(1a_2)^{-1}$, or peak 3 in Fig. 1. However, the major increase in $\sigma(O_2^+/O_3)$ in both data sets from ∼8 to 21 Mb between ∼14 and 16.5 eV, does not have a counterpart in the photoelectron spectrum. One possible explanation is absorption to super-excited states which autoionize partly to stable states (forming O_3^+) but mostly to dissociating ionic states (forming O_2^+). In the photoabsorption/photoionization figure of Cook [23] there is a marked increase in photoabsorption cross section between 14 and 16 eV, but the quantum yield stays below unity, suggesting that some of these super-excited states predissociate.

The $\sigma(O^+/O_3)$ spectra in Fig. 5 overlap well above 17 eV, but suggest anomalous structure at lower energy in the Mocellin data as these authors imply. Rather than there being a prominent increase in signal after 18.3 eV (Mocellin et al.) there appears to be a slow growth from a delayed threshold, as would be anticipated by QET for a second fragment competing with an advantaged phase space from the first fragment. There is no obvious correlation with the photoelectron spectrum of Fig. 1.

4. Conclusions

As regards the photoelectron spectrum of ozone, it has been abundantly pointed out since 1975 that a single configuration Hartree–Fock description is totally inadequate. Koopmans' theorem is doubly violated. Reference is made to a recent CI description. The energy dependence of the absolute partial cross sections of the various ionic states is not known experimentally. The only available calculated ones cannot be expected to closely represent experimental partial cross sections, since they would require large scale CI. Insofar as we have any handle on the total ionization cross-section, it disagrees in shape and magnitude with the calculation. Nevertheless, in the absence of any experimental branching ratios or partial cross sections, we reproduce the calculated ones of Padial et al. [21] having taken notice of their shortcomings.

For the absolute partial cross sections of the ions, the experimental situation is more optimistic. Only one absolute total photoionization cross-section measurement is known, and requires correction according to sum rule analysis [24]. Two photoionization mass spectrometric investigations are known, with apparently discordant results. However, by an eclectic choice of parameters, it is possible to assemble a plausible set of absolute partial cross sections for O_3^+, O_2^+ and O^+ from ozone. Upon comparing these cross sections with the photoelectron spectrum, it becomes apparent that a major increase in O_2^+ (and some in O_3^+) is not accounted for in the photoelectron spectrum and consequently autoionization is invoked. Quasiequilibrium theory (QET) rather than orbital character (bonding/anti-bonding) appears to explain the shape of the O^+ partial cross section and its retarded onset. On the other hand, the increase in O_3^+ after the appearance of the first fragment O_2^+ would appear to violate a simple form of QET.

Acknowledgments

This work was supported by the US Department of Energy, Office of Basic Energy Sciences, under Contract No. DE-AC02-06CH11357.

References

[1] J.-M. Colmont, J. Demaison, J. Coléou, J. Mol. Spectrosc. 171 (1995) 453.
[2] P.J. Hay, T.H. Dunning Jr., W.A. Goddard III, J. Chem. Phys. 62 (1975) 3912.
[3] W.D. Laidig, H.F. Schaeffer III, J. Chem. Phys. 74 (1978) 3411.
[4] S. Stranges, M. Alagia, G. Fronzoni, P. Decleva, J. Phys. Chem. A105 (2001) 3400.
[5] N.J. Mason, J.M. Gingell, J.A. Davies, H. Zhao, I.C. Walker, M.R.F. Siggel, J. Phys. B 29 (1996) 3075.
[6] L.T. Molina, M.J. Molina, J. Geophys. Res. 91 (D13) (1986) 14501.
[7] K. Takahashi, N. Taniguchi, Y. Matsumi, M. Kawasaki, M.N.R. Ashfold, J. Chem. Phys. 108 (1998) 7161.

[8] K. Wiesner, R.F. Fink, S.L. Sorensen, M. Andersson, R. Feifel, I. Hjelte, C. Miron, A. Naves de Brito, L. Rosenqvist, H. Wang, S. Svensson, O. Björneholm, Chem. Phys. Lett. 375 (2003) 76.
[9] S. Katsumata, H. Shiromaru, T. Kimura, Bull. Chem. Soc. Jpn. 57 (1984) 1784.
[10] J.M. Dyke, L. Golob, N. Jonathan, A. Morris, M. Okuda, J. Chem. Soc., Faraday Trans. 70 (2) (1974) 1828.
[11] T. Schmelz, G. Chambaud, P. Rosmus, H. Köppel, L. Cederbaum, H.-J. Werner, Chem. Phys. Lett. 183 (1991) 209.
[12] H. Müller, H. Köppel, L.S. Cederbaum, J. Chem. Phys. 101 (1994) 10263.
[13] A.J. McKellar, D. Heryadi, D.L. Yeager, T.A. Nichols, Chem. Phys. 238 (1998) 1.
[14] N. Kosugi, H. Kuroda, S. Iwata, Chem. Phys. 58 (1981) 267.
[15] H. Couto, A. Mocellin, C.D. Moreira, M.P. Gomes, A. Naves de Brito, M.C.A. Lopes, J. Chem. Phys. 124 (2006), 204311-1.
[16] S. Willitsch, F. Innocenti, J.M. Dyke, F. Merkt, J. Chem. Phys. 122 (2005), 024311-1.
[17] M.J. Weiss, J. Berkowitz, E.H. Appelman, J. Chem. Phys. 66 (1977) 2049.
[18] J.T. Moseley, J.B. Ozenne, P.C. Cosby, J. Chem. Phys. 74 (1981) 337.
[19] Y. Ohtsuka, J. Hasegawa, H. Nakatsuji, Chem. Phys. 332 (2007) 262.
[20] P. Decleva, G. De Alti, A. Lisini, J. Chem. Phys. 89 (1988) 367.
[21] N. Padial, G. Csanak, B.V. McKoy, P.W. Langhoff, J. Chem. Phys. 74 (1981) 4581.
[22] G.R. Cook, Trans. Am. Geophys. Union 49 (1968) 736A.
[23] G.R. Cook, in: K. Ogata, T. Hayakawa (Eds.), Recent Developments in Mass Spectrometry, University Park Press, Baltimore, 1970, p. 761.
[24] J. Berkowitz, Atomic and Molecular Photoabsorption. Absolute Total Cross Sections, Academic Press, London, 2002, p. 228.
[25] R.J. Celotta, S.R. Mielczarek, C.E. Kuyatt, Chem. Phys. Lett. 24 (1974) 428.
[26] M. Ogawa, G.R. Cook, J. Chem. Phys. 28 (1958) 173.
[27] N. Padial, G. Csanak, B.V. McKoy, P.W. Langhoff, Phys. Rev. A 23 (1981) 218.
[28] N. Taniguchi, K. Takahashi, Y. Matsumi, S.M. Dylewski, J.D. Geiser, P.L. Houston, J. Chem. Phys. 111 (1991) 6350.
[29] F. Merkt, R. Signorell, H. Palm, A. Ostserwalder, M. Sommavilla, Mol. Phys. 95 (1998) 1045.
[30] C.E. Moore, Atomic Energy Levels, NSRDS-NBS 35, vol. 1 (1971).
[31] K.A. Newson, S.D. Price, Int. J. Mass Spectrom. 153 (1996) 151.
[32] A. Mocellin, K. Wiesner, F. Burmeister, O. Björneholm, A. Naves de Brito, J. Chem. Phys. 115 (2001) 5041.